Ionospheric Storm Effects in GPS Total Electron Content

Evan G. Thomas[1], Joseph B. H. Baker[1], J. Michael Ruohoniemi[1], and Anthea J. Coster[2]

[1]Virginia Tech
1901 Innovation Drive
Blacksburg, VA 24060
USA

[2]MIT Haystack Observatory
Off Route 40
Westford, MA 01886
USA

ABSTRACT

Total electron content (TEC) is a commonly-used parameter for characterizing the Earth's ionosphere. It is defined as the total number of electrons within a cross-sectional volume along a path between two points and given in units of 1×10^{16} electrons/m^2, or 1 TECU. Ionospheric TEC measurements can be obtained from the pseudorange and carrier-phase data contained in the L1 (1575.42 MHz) and L2 (1227.60 MHz) signals broadcast by Global Positioning System (GPS) spacecraft and recorded by a ground-based receiver. By collecting data from the thousands of stationary GPS receiver sites around the world, globally-gridded maps of GPS TEC allow for imaging of large-scale ionospheric electron density structures at high spatial and temporal resolution. Strong gradients associated with the edges of these density structures have been related to outages of aircraft navigation services and disruption of satellite communication links. We present an analysis of ionospheric GPS TEC variations driven by geomagnetic storms during the current solar cycle (2010–2013) with the aim of improving existing space weather modeling and forecasting capabilities.

1. INTRODUCTION

A geomagnetic storm is characterized by a disturbance in the horizontal (*H*) component of the Earth's magnetic field at the equator due to the changing intensity of the ring current [*Gonzalez et al.*, 1994]. This modification of the ring current intensity is attributed to increased coupling between the solar wind and magnetosphere, which for a storm is often driven by either a coronal mass ejection (CME) or co-rotating interaction region (CIR). The Disturbance storm time (*Dst*) index is an hourly measure of the average global *H* variation obtained from low-latitude ground magnetometer stations and has traditionally been used to identify geomagnetic storm intervals.

Many storms exhibit three distinct phases: an initial phase when increased pressure in the solar wind compresses the magnetosphere (often resulting in a positive increase in *Dst*), followed by the main phase when a southward turning of the interplanetary magnetic field (IMF) and increased solar wind-magnetosphere coupling leads to ring current intensification (and a sharp decrease of *Dst* to negative values), and finally a recovery phase where the system slowly returns to its pre-storm state over several hours or days [*Hutchinson et al.*, 2011]. The magnitude of the *Dst* decrease and durations of each of these storm phases can vary quite significantly from one event to another.

The ionosphere, a region of weakly ionized plasma which stretches from about 50 km to 1,000 km above the Earth's surface, responds to the varying solar and magnetospheric energy inputs associated with geomagnetic storms [*Buonsanto*, 1999]. The ionosphere is divided into three principal layers based on the altitude profile of electron density: the *D* region (below 90 km), *E* region (between 90 km and 130 km), and *F* region (above 130 km). The primary source of ionization in the dayside upper atmosphere is photoionization by solar EUV radiation. In the *F* region, where electron densities reach a maximum, production is mainly controlled by photoionization of atomic oxygen while loss is mostly due to a two-step process of charge transfer with molecular nitrogen and oxygen and subsequent dissociative recombination.

The ionospheric electron density response to a geomagnetic storm is traditionally classified as either a positive (increase) or negative (decrease) storm effect. Initial positive storm effects are attributed to an uplift in the ionospheric *F* layer to regions of decreased recombination by electric fields of magnetospheric origin and travelling atmospheric disturbances (TADs). The following longer-lived negative storm effects are attributed to neutral composition changes expanding equatorward from composition disturbance zones, specifically an increase in molecular gas [O_2, N_2] and decrease in atomic oxygen [O] density [*Fuller-Rowell et al.*, 1994; *Prölss*, 1995].

One increasingly popular approach for describing ionospheric behavior uses measurements of vertically-integrated total electron content (TEC) from ground-based Global Positioning System (GPS) receivers [*Mendillo*, 2006]. The goal of this study is to statistically examine positive and negative ionospheric storm effects at high spatial and temporal resolution using the densely-populated network of GPS receivers in North America. We present first results from a superposed epoch analysis of these storm-time TEC variations.

2. METHODOLOGY

Using *Dst* values from the World Data Center for Geomagnetism in Kyoto, we have manually identified all geomagnetic storms during the current solar cycle maximum (2010–2013) which reached a magnitude of at least -40 nT. The time of storm main phase onset (sharp decrease to negative *Dst* values) has been selected as the beginning of each geomagnetic storm for the superposed epoch approach. More precise onset times are determined using the one-minute Sym-H index, which has been shown to closely track the hourly *Dst* index for events with magnitude ≤ -300 nT [*Wanliss and Showalter*, 2006]. A total of 69 geomagnetic storms with *Dst* ≤ -40 nT were identified during the 4-year period; Table 1 shows the distribution of these events by season and magnitude.

Season		**Magnitude**
Winter: 9	Summer: 19	-80 < *Dst* ≤ -40 nT : 50
Spring: 24	Fall: 17	*Dst* ≤ -80 nT : 19

Table 1. Distribution of geomagnetic storm events by season and *Dst* magnitude.

Global maps of GPS TEC binned into 1°×1° cells at 5 min cadence are obtained from the online Madrigal database at MIT Haystack Observatory [*Rideout and Coster*, 2006]. One TEC unit (TECU) is given as 1×10^{16} electrons/m^2 and represents the total number of electrons contained in a column extending through the ionosphere with a cross-sectional area of 1 m^2. For this study, the original 5 min GPS TEC values over North America are re-binned from the 1°×1° geographic latitude and longitude cells onto a new 2°×4° grid using 30 min average values. This decrease in

temporal resolution still represents an improvement over previous studies using TEC maps with 2 hr cadence.

Instantaneous (TEC) and 27-day median "quiet" (TECq) values were recorded from the new 30-min latitude/longitude grid for the interval ranging from 1 day before to 3 days after each of the 69 storm main phase onset times. Similar to *Biqiang et al.* [2007], these values were then used to calculate the storm-time change in total electron content (RTEC) as

$$RTEC = (TEC - TECq)/TECq$$

These TEC variations were then organized by magnetic latitude (MLAT) and magnetic local time (MLT) for each event. Finally, median values of RTEC within each MLAT/MLT bin were calculated using the available data from all storm events. Here we use a relative change (RTEC) rather than an absolute difference because of the dependence of the background TEC magnitude on solar cycle and diurnal variability. Note that we have also not separated storm events by magnitude or season due to the relatively small number of total events in each category.

3. RESULTS

Here we present a subset of results from the superposed epoch analysis described above. Figure 1 is a keogram showing median RTEC values along the 12 MLT (noon) meridian versus magnetic latitude. Bins with no data have been shaded gray to differentiate from the case of no change in TEC. Almost immediately following the storm main phase onset (vertical dashed line), positive RTEC values are observed across all latitudes in the North American sector. A transition to sustained negative RTEC begins at higher latitudes within 6 hours of storm onset; the changeover from positive to negative TEC response is completed at all latitudes within 18 hours after onset. This longer-lasting negative phase is observed to persist for at least the next 36 hours.

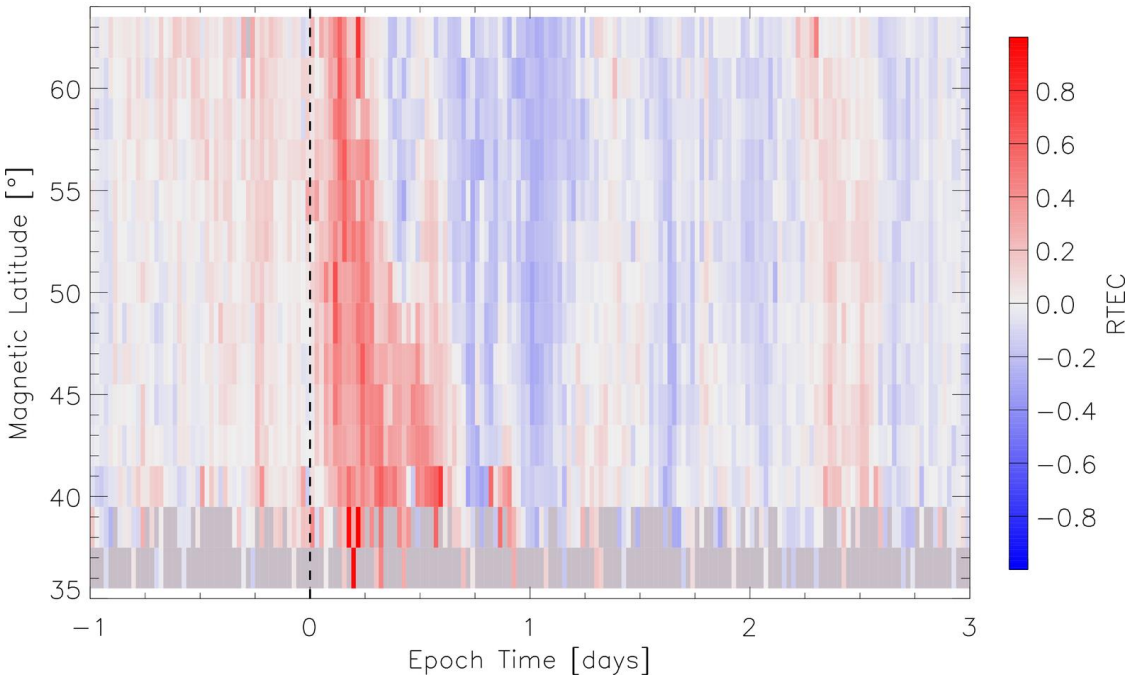

Figure 1. Keogram of median TEC storm-time deviation (RTEC) for all 69 geomagnetic storm events at 12 MLT (noon) versus geomagnetic latitude. Vertical dashed line indicates storm main phase onset; regions with no data have been shaded gray to differentiate from case of RTEC=0.

Next we examine the storm-time TEC variations along the 18 MLT (dusk) meridian. Figure 2 shows median RTEC values in this MLT sector in the same format as Figure 1. Similar to the results for 12 MLT, a strong positive response is observed immediately following storm onset. Here the negative response at higher latitudes begins even sooner and follows a much clearer progression to lower latitudes in the first 4-20 hours after storm onset. The magnitude of this negative response is greatest at higher latitudes, and when viewed on a global scale appears similar in structure to the midlatitude density trough [*Halcrow and Nisbet*, 1977]. In contrast to the storm response at noon, the negative storm phase appears simultaneously at all latitudes below the trough approximately 24 hours after onset. The somewhat recurrent positive RTEC signatures located at 36 and 60 hours after storm onset are a possible artifact of averaging across storms with varying phase durations and are under further investigation.

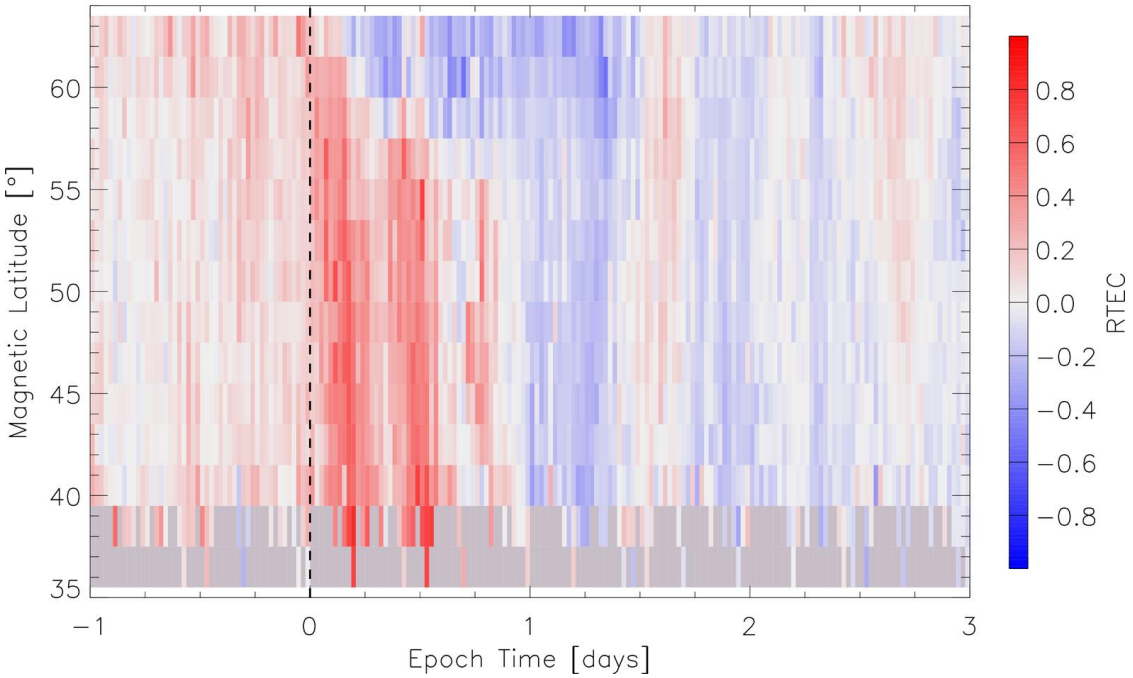

Figure 2. Keogram of median TEC storm-time deviation (RTEC) for all 69 geomagnetic storm events at 18 MLT (dusk) versus geomagnetic latitude in the same format as Figure 1.

4. CONCLUSIONS

We have performed a superposed epoch analysis of the ionospheric TEC response in the North American sector to 69 geomagnetic storms from the recent solar cycle maximum (2010–2013). Median storm-time variations in the 12 MLT (noon) and 18 MLT (dusk) sectors have been presented and are largely consistent with previous global studies using much coarser spatial and temporal averaging [*Biqiang et al.*, 2007]. While the evolution of the midlatitude density trough was visible (Figure 2), there were no obvious signatures of storm enhanced density (SED) plumes. Results were also obtained for all other MLT sectors but are not included here.

By focusing on the North American region we have tried to avoid mixing storm-time variations with universal time (UT) effects due to the offset between Earth's geographic and magnetic poles. Seasonal effects have not yet been examined due to the uneven distribution of storm events during the interval of study; future work will include all storm events with $Dst \leq$ -40 nT from a longer period with sufficient TEC availability (2001-2013) to address this issue. Finally, we also plan to account for the variability in storm main phase and recovery phase durations in our analysis.

ACKNOWLEDGMENTS

The authors from Virginia Tech are funded by NSF Award Numbers AGS-0838219 and AGS-1243070. A. J. C. is funded by NSF Award Numbers ATM-1141923 and AGS-1243058.

REFERENCES

Biqiang, Z., W. Weixing, L. Libo, and M. Tian (2007), Morphology in the total electron content under geomagnetic disturbed conditions: Results from global ionosphere maps, *Ann. Geophys.*, 25, 1555-1568.

Buonsanto, M. J. (1999), Ionospheric Storms – A Review, *Space Sci. Rev.*, 88, 563-601.

Fuller-Rowell, T. J., M. V. Codrescu, R. J. Moffett, and S. Quegan (1994), Response of the thermosphere and ionosphere to geomagnetic storms, *J. Geophys. Res.*, 99(A3), 3893-3914.

Gonzalez, W. D., J. A. Joselyn, Y. Kamide, H. W. Kroehl, G. Rostoker, B. T. Tsurutani, and V. M. Vasyliunas (1994), What is a geomagnetic storm?, *J. Geophys. Res.*, 99(A4), 5771-5792.

Halcrow, B. W., and J. S. Nisbet (1977), A model of F2 peak electron densities in the main trough region of the ionosphere, Radio Sci., 12(5), 815-820.

Hutchinson, J. A., D. M. Wright, and S. E. Milan, Geomagnetic storms over the last solar cycle: A superposed epoch analysis, *J. Geophys. Res.*, 116, A09211.

Mendillo, M. (2006), Storms in the ionosphere: Patterns and processes for total electron content, *Rev. Geophys.*, 44, RG4001.

Prölss, G. W. (1995), Ionospheric F-region storms, in *Handbook of Atmospheric Electrodynamics*, vol. 2, edited by Hans Volland, chap. 8, 195-228.

Rideout, W., and A. Coster (2006), Automated GPS processing for global total electron content data, *GPS Solutions*, 10(3), 219-228.

Wanliss, J. A., and K. M. Showalter (2006), High-resolution global storm index: Dst versus SYM-H, *J. Geophys. Res.*, 111, A02202.